Supplement of Clim. Past, 21, 517–528, 2025
https://doi.org/10.5194/cp-21-517-2025-supplement

Climate of the Past
Open Access
EGU

Supplement of

Total air content measurements from the RECAP ice core

Sindhu Vudayagiri et al.

Correspondence to: Thomas Blunier (blunier@nbi.ku.dk)

Contents

S1 PICE TAC system

The set up consists of 3 extraction chambers connected to a differential pressure gauge via an extraction line (¼" stainless steel tube) that is separated into various sections by stainless steel bellows sealed valves (Swagelok, SS-4H) (Aagaard, 2015, Fig. S1). The samples are placed in extraction chambers that can be vacuum sealed and attached to the extraction line via Swagelok VCR fittings. The extraction chambers (Fig. S2) are made of aluminium with outer dimensions of 42 x 60 x 60 mm and inner dimensions of 32 x 32 x 32 mm. The chambers are designed with rounded edges and the bottom floor inside the chamber has 3 little bumps of 1mm in height to prevent any air from getting trapped below the ice sample. The chambers can be cooled or heated from the bottom upwards by placing them on a base fitted with Peltier plates. The extraction line is under vacuum which is maintained with the help of a vacuum pump (Pfeiffer DUO 3 M, DN 16 KF). The differential pressure gauge (DPG) used is P-BADP/P-BADR, Smart/HART pressure transmitter that can measure a differential pressure of 0.1 kPa to 10 MPa with an accuracy of ± 0.075%. The extraction line has a water vapor trap followed by a HayeSep trap (HayeSep D 20/40 mesh). An extra volume is also provided in the measuring area for increasing the measuring volume if needed.

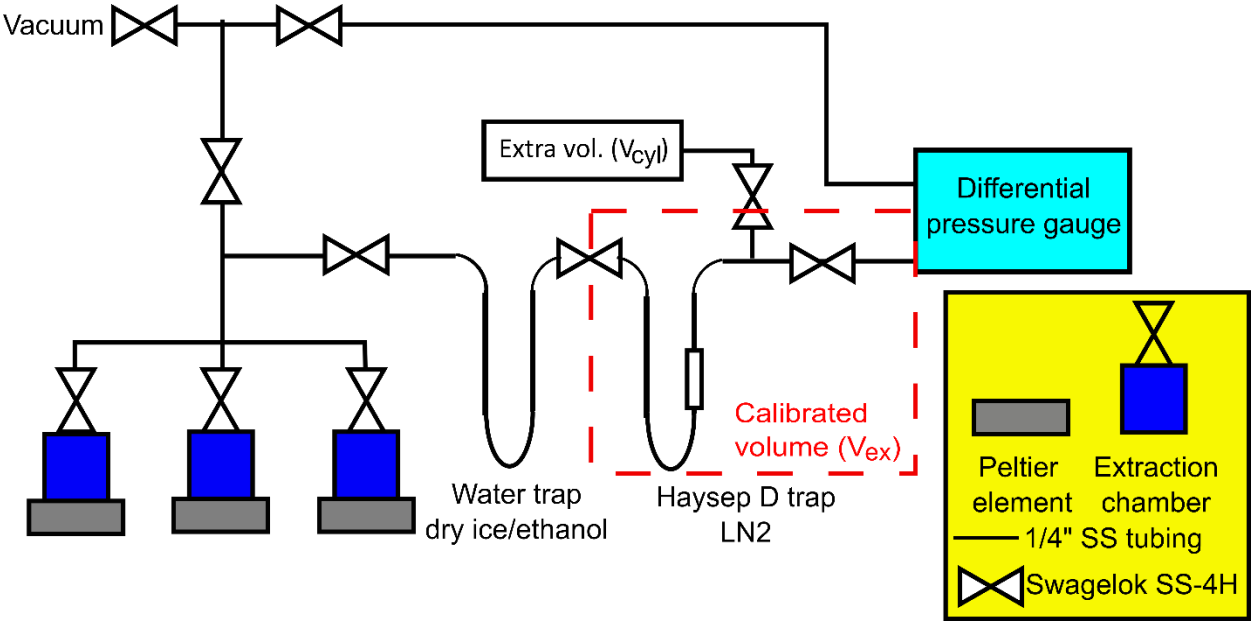

Figure S1: Schematic representation of the vacuum volumetric set-up for measuring the air content in discrete ice core samples.

Cubical samples (~ 22 x 25 x 25 mm), weighing ~ 10 to 15 g each, are cut at specific depths of the ice core (Fig. S4). The cut samples are then photographed, weighed and the dimensions measured accurately. Each ice sample is placed inside a pre-cooled chamber and sealed airtight by fastening the 8 screws on the lid along with an O-ring (NBR 70) between the lid and the chamber. The chambers are then connected to the set up via VCR connections and kept cold by the Peltier plates (Adaptive PE-127-20-15) upon which they are placed. The chambers with ice samples are evacuated for 30 minutes. During the 30-minutes evacuation the samples sublimate leading to a systematic offset of all TAC measurements that we do not correct for. Lipenkov et al. (1995) estimate the mass loss to 1% in their original system. The chambers are then sealed off and the ice samples are melted and re-frozen with the help of the Peltier plate. The gas released from the sample is transferred through a water trap cooled by dry ice/ethanol onto a HayeSep trap held at LN_2 temperature. A small percentage of gas remains dissolved in the frozen meltwater. Therefore, another melt-refreezing cycle is used to collect a maximum of the gas from the sample. By heating the HayeSep trap, the captured gas is released into the calibrated measuring volume (Fig. S1) and its pressure is measured by the differential pressure gauge together with the room temperature.

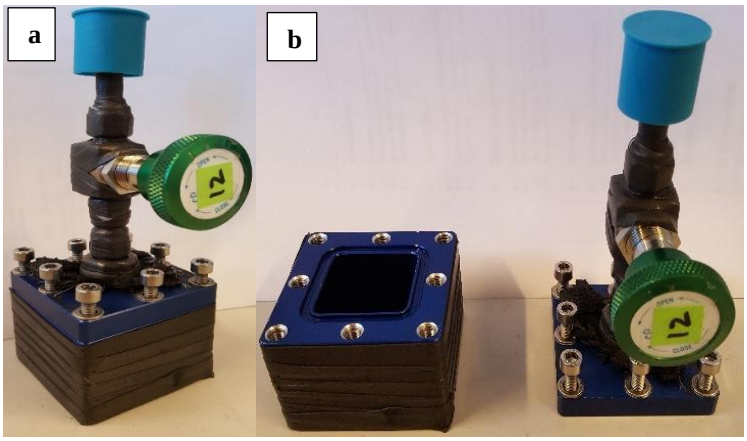

Figure S2: (a) Extraction chamber and (b) chamber with open lid.

The DPG is calibrated by attaching an absolute pressure gauge to the set-up following the procedure detailed in the thesis of Johanne Aagaard (2015).

The measuring volume (V_{ex}) must be determined accurately for precise TAC calculations. We follow the method developed by Schwander (1984) also described in Lipenkov et al. (1995). For determining the V_{ex} precisely, steel balls of different known volumes (B) are placed in the extraction chamber, thereby changing the volume of the set-up. Dry air is admitted into the set up and is captured in the extra volume (V_{cyl}) with pressure P1. The rest of the set-up is evacuated. The air in V_{cyl} is then expanded to fill out V_{ex} and the pressure is noted as P2. Then the air is expanded to the entire volume of the set-up (V_t) with pressure noted as P3. The relation of these pressures and volumes lead to the following equation (S1).

$$B = V_t - V_{ex}\frac{P_2}{P_3} \quad \text{(S1)}$$

The pressures are measured with different combinations of steel balls in the extraction chamber (Fig. S2). From the linear regression (Fig. S3), V_{ex} is determined as 159.68 cm^3. The standard error of the regression gives an uncertainty of ± 0.068 cm^3 for V_{ex}.

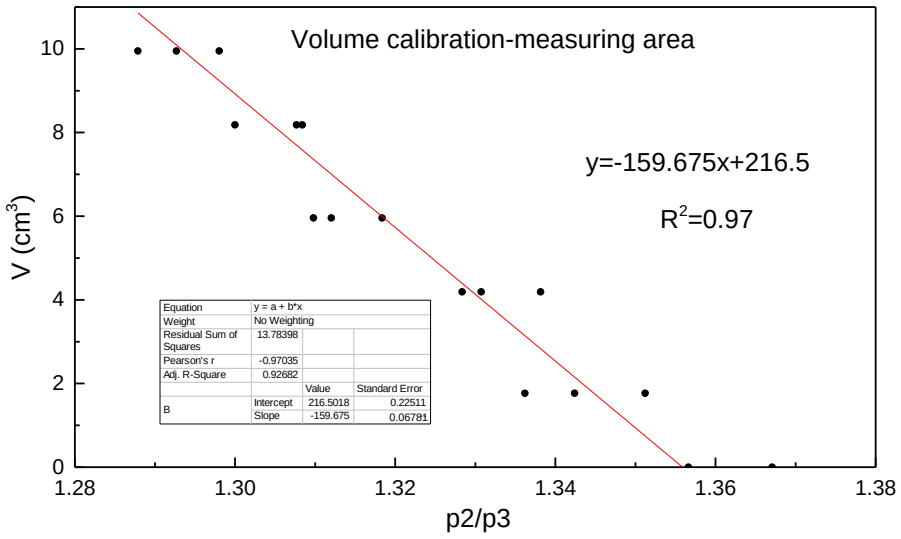

Figure S3: Volume Calibration: Volume (B) taken up by calibration volumes (steel balls) versus pressure ratio before and after expansion. The slope of the regression equals the size of the measuring volume.

S2 SPIDER-System calibration

Careful calibration is essential for accurate sample measurement. Calibration here involved measuring the volume of the sampling lines and the effective temperature of the system (Fegyveresi, 2015). Both experiments made use of the ideal gas law relating pressure, volume, and temperature in the system. The volume of each of the 14 individual system lines ($V_{line(s)}$) was first experimentally determined. Steel plugs (inserts) with known volumes (~57 cm^3, based on m_{steel} and ρ_{steel} for each plug) chosen to approximate ice samples, were inserted into each of the empty vessels (also with known volumes of ~96 cm^3). An isothermal experiment for each of the vessels and lines individually was initiated, as follows: 1) gas pressure was measured in the vessel system line with the vessel valves closed; 2) the system was evacuated for 30 minutes, removing all air from the system lines (< $4x10^{-4}$ torr) while leaving air within the headspace of the vessel; 3) valves were then opened, allowing the headspace air to expand into the system lines where the final pressure (P_{final}) was measured. The volume of the line for each vessel (V_{line}) can then be determined from,

$$V_{line} = \frac{(V_{vessel} - V_{steel})(P_{initial} - P_{final})}{P_{final}} \quad \text{(S2)}$$

Laboratory temperatures may change by a few degrees from day to day and throughout the run due to excessive heat generated by the chiller. As the room temperature influences the temperature of the extraction manifold and GC sample loop, we need to determine the effective temperature of the line when air samples are analysed. To calibrate this, three expansion experiments were run for each vessel individually, with the vessel held at -70°C as during sampling, and with the room temperature at 24.05, 28.45, and 31.35°C. Each of these three runs for each vessel yielded an effective temperature (T_{eff}),

$$T_{eff} = \frac{P_{final}(V_{head} - V_{line})T_{initial}}{P_{initial}V_{head}} \quad \text{(S3)}$$

Substituting V_{head} for V_{vessel}- V_{steel} yields,

$$T_{eff} = \frac{P_{final}(V_{vessel} - V_{steel} + V_{line})T_{initial}}{P_{initial}(V_{vessel} - V_{steel})} \quad \text{(S4)}$$

Linear regressions for T_{eff} versus room temperature for each vessel was calculated, and these equations were then used with measured room temperature when the sample was expanded into the manifold to reduce sample data to standard temperature and pressure (STP; Eqs. S5 and S6).

$$V_{STP} = \left(\frac{P_{final}V_{final}}{T_{eff}}\right)\left(\frac{T_{STP}}{P_{STP}}\right) \quad \text{(S5)}$$

$$TAC = \frac{V_{STP}}{\mathrm{m}_{ice}} \quad \text{(S6)}$$

For further detailed information on the calibration of the SPIDER extraction device, refer to the thesis of John M. Fegyveresi (Fegyveresi, 2015).

For $\delta^{15}N$ the measurement procedure is similar. However, the samples are only 13g on average. Due to the relatively large headspace compared to the sample size, the solubility correction becomes negligible.

S3 Cut bubble correction

The cut bubble effect (CBE) calculates from the average bubble diameter $\langle D \rangle$ in the sample and sample surface area A_S and volume V_S, respectively (Martinerie et al., 1990). The calculation assumes spherical bubbles.

$$CBE = \frac{TAC - TAC_{raw}}{TAC} = \frac{1}{2}\langle D \rangle \frac{\mathrm{A}_S}{V_S} \quad \text{(S7)}$$

CBE corrected total air content (TAC) then calculates from the TAC_{raw}

$$TAC = (1 - CBE)^{-1} \cdot TAC_{raw} \quad \text{(S8)}$$

Samples measured at PICE are corrected individually. Sample size is measured to 0.5 mm precision. A photograph of each sample is taken (Fig. S4) from which an average of 20 bubble diameters, measured with a calliper, is taken as the sample bubble diameter.

Figure S4: Picture of sample from RECAP bag 946 (2.2 x 2.2 x 2.4 cm) used to determine the average bubble diameter.

Individual bubble diameters have not been measured for samples measured at PSU. Those measurements are a by-product of CH_4 concentration and $\delta^{15}N$ measurements. Bubble diameters are estimated from the PICE data. The bubble diameter decreases linearly from 120 to 530 m below surface (Fig. S5). For the corresponding sample range in the PSU data (from the surface to the YD-Preboreal transition at 532.6 m below surface) we calculate the bubble diameter from the linear regression of the PICE data. The one sigma prediction interval has an uncertainty of 0.07 mm calculated with the MATLAB function "predint". The bubble diameter below

530 m is very variable, and we apply the average bubble size of the PICE data (N = 88) which is 0.362 mm ± 0.114 mm (one sigma standard deviation).

The resulting cut bubble effect (CBE) depends on the size and shape of the sample. Samples from PSU-CH_4 measurements are cylindrical with diameter 4.1 cm, height of 5.5 ± 0.3 cm, and weighing 65 ± 3 g each. PSU-$\delta^{15}N$ samples are smaller cubes of 20 x 12 x 50 mm weighing 13 g. Averaged CBE corrections in table S1.

	Upper section (above 532.6 m)	Lower section (below 532.6 m)
PSU-CH_4 samples	1.7 ± 0.5%	2.4 ± 0.8%
PSU-$\delta^{15}N$ samples	4.2 ± 1.1%	5.6 ± 1.8%

Table S1: Average CBE corrections for the different sections and samples of the PSU data.

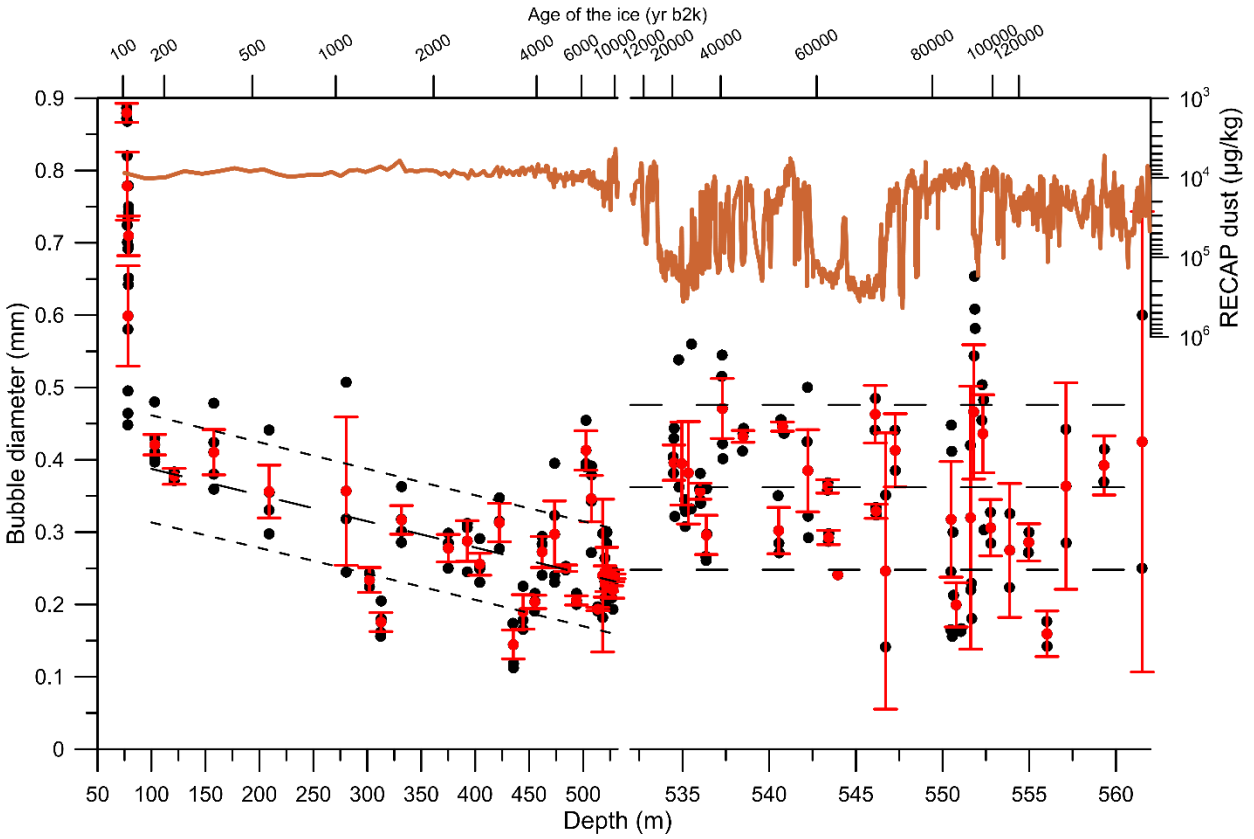

Figure S5: Bubble diameter of the PICE samples versus depth. Black dots are individual samples. Red dots with error bars are averages for samples within one bag (0.55 cm) with standard errors of the mean. Dotted lines are one sigma error estimates for the correction of the PSU samples. Red line, RECAP dust record for orientation (Simonsen et al., 2019). Top axis is the ice time scale for the RECAP core (Simonsen et al., 2019).

S4 Agreement between datasets

At PICE, the air from the ice samples is extracted with two melt-freeze cycles and is stripped off its moisture before its pressure is measured. The extraction process at PSU has only one melt-freeze cycle and there is no water vapor

trap leading to considerable uncertainty due to the added partial pressure of the moisture. Further CBE is not measured on these samples but estimated from the PICE measurements (see section S3).

To assess the quality of the data sets, we present correlation plots between the PSU and the PICE datasets. Figure S6 shows average values for the two PSU datasets versus their closest, (within one meter) average correspondent in the PICE dataset. Samples that have no correspondent within 1 meter distance are excluded. Offsets of individual samples can be large. However, we observe no systematic offset between the datasets.

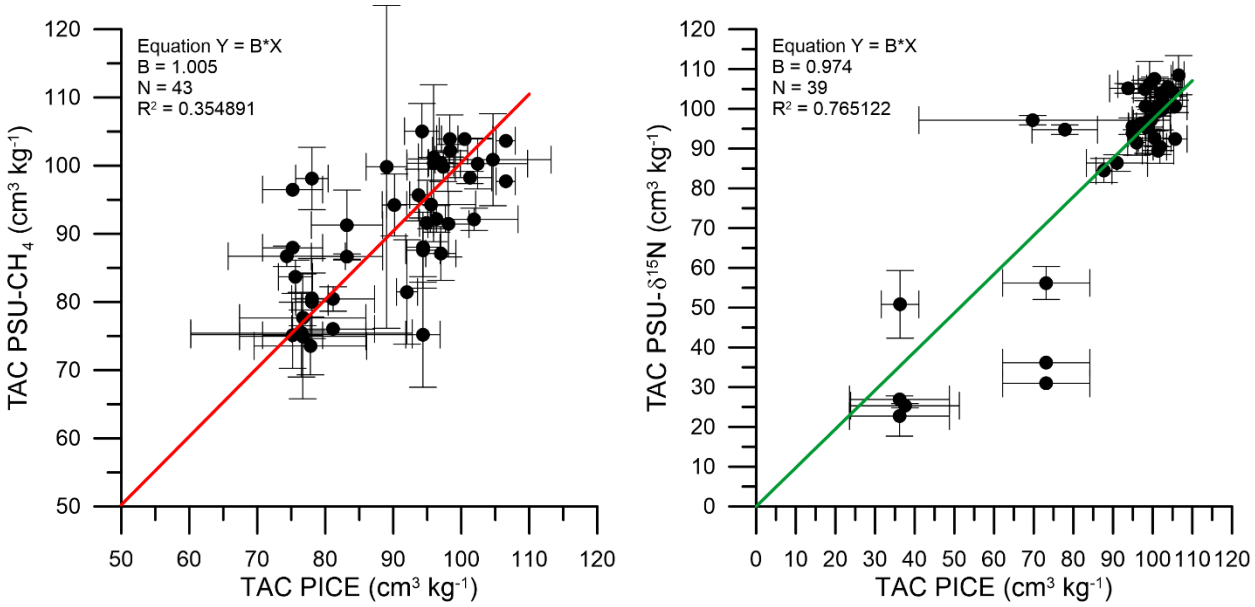

Figure S6: Correlation of PSU and PICE TAC data. Plotted are the closest PICE neighbours (within one meter) to the PSU TAC data obtained during the CH_4 and $\delta^{15}N$ measurements on the left- and right-hand side, respectively. Uncertainties are standard errors of the mean data.

S5 Time scale

We are making use of the RECAP GICC05 ice age scale (Simonsen et al., 2019). The time scale is based on counting annual layers in the upper section and by tie points to other Greenland ice cores in deeper strata (see Simonsen et al., 2019 for details). Note that all data are presented on the ice time scale in our manuscript.

The gas time scale is younger by Δage, which is variable depending on temperature and accumulation rate.

Firn air measurements from RECAP show the kink in the CO_2 and $\delta^{15}N$ records indicating the close off depth at about 55.5 m below surface. This results in a shallow Δage of only about 75 years. In the glacial Δage is quite variable. From matching D-O events in the water isotopes to their corresponding CH_4 signal, Δage is about 700 years with a large standard deviation of roughly 250 years (Individual Δage values are shown in Fig. S9 a-d).

S6 Theoretical present-day TAC with 0% and 100% melt layers

S6.1 Theoretical present-day TAC of ice unaffected by melt at Renland ice cap

Unfortunately, no data is available for the present day annual mean pressure at the Renland ice cap. Therefore, we calculate it by applying the barometric formula (equation 2). The closest measurement station is Illoqqortoormiut

which we use as the reference station with T_a= -7.5°C, h_a= 0 m, P_a = 1012.2 mbar (Cappelen et al., 2001). We use the Renland bore hole temperature T_c = -17.8°C, h_c = 2315 m, M_{air} = 0.028964 kg/mol. The present day annual mean lapse rate can be calculated from the temperatures at Renland and Illoqqortoormiut, respectively to -4.5 °C km^{-1}. The average pressure then calculates to 747 mbar. We calculate the pore volume V_c according to Martinerie et al. (1994) at T_c = -17.8°C to 134 cm^3 kg^{-1}. TAC then calculates (equation 1) to 99 cm^3 kg^{-1} at standard temperature and pressure. This value compares well to the TAC measured for the last 2000 years (depth range 76.6 - 345.7 m, Fig. S7).

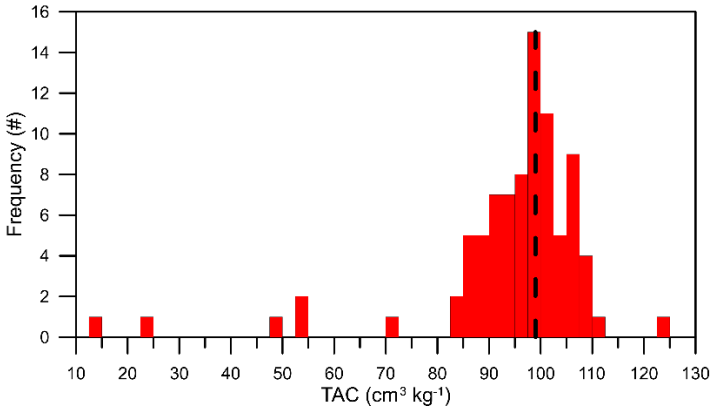

Figure S7: TAC of individual samples in the depth range 76.6 to 345.7m covering the last 2000 years. Note samples with known melt features are included. Black hashed line indicates the theoretical calculated air content of 99 cm^3 kg^{-1}.

S6.2 Theoretical present-day TAC in a 100% melt sample at the Renland ice cap

For this calculation we assume that the melt water of the sample is in equilibrium with the atmosphere and then freezes instantly. To compute the amount of air dissolved in water at 0°C and at an atmospheric pressure of 747 mbar, Henry's solubility law will be used (Sander, 2015).

Temperature dependence of Henry's constant,

$$H^{cp}(T) = H_{\Theta}^{cp} \times exp\left[\frac{-\Delta_{sol}H}{R}\left(\frac{1}{T} - \frac{1}{T^0}\right)\right]$$

The concentration of gas dissolved in mol m^{-3} calculates to $C_a = H_{\Theta}^{cp} \times P$, where P is the partial pressure of the species in the gas phase at equilibrium conditions, in this case on Renland.

TAC for an individual gas calculates as $TAC = \frac{C_a \times R \times T_0}{\rho_{H2O} \times p_0}$, with T_0 = 273.15 K and p_0 = 1013mbar.

Gas	H_{Θ}^{cp} $(\frac{mol}{Pa.m^3})$ (Θ = 298.15 K)	$\frac{-\Delta_{sol}H}{R}$ (K)	C_a $(\frac{mol}{m^3})$ at 0°C	C_a $(\frac{mol}{m^3})$ at 2°C
O_2	1.3×10^{-5}	1700	0.344	0.328
N_2	6.4×10^{-6}	1600	0.617	0.591
			TAC 21.5 cm^3 kg^{-1}	**TAC 20.6 cm^3 kg^{-1}**

Table S1, Constants and calculation for TAC of melt water fully equilibrated with the atmosphere at Renland altitude at 0 and 2°C.

From the theoretical TAC calculations for no melt and 100% melt at present day Renland we obtain: melt-% $= -1.291 \cdot TAC\ (cm^3\ kg^{-1}) + 127.819$ (Fig. S8). Samples from bag no. 143 of the RECAP ice core were cut so that they have approximately 50% and 100% melt. This approach has obviously a large uncertainty. Nevertheless, the results are also shown in Fig. S8, validating our theoretical approach.

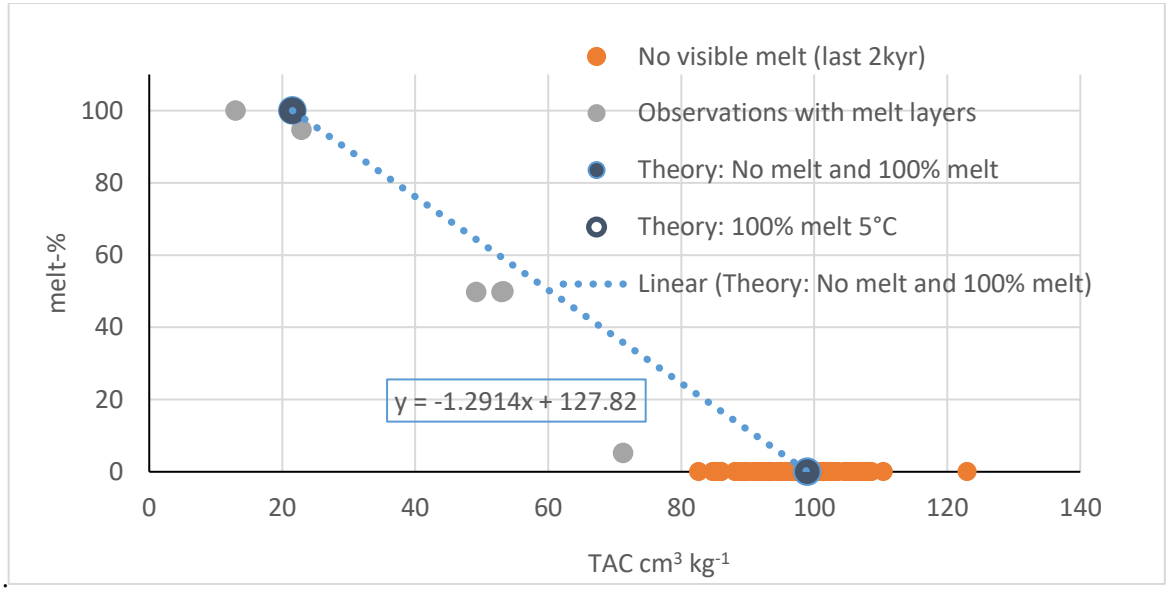

Figure S8: Data and theoretical values for TAC with varying contributions from melt layers.

S7 The glacial record of RECAP and NGRIP

The records are presented in 4 sections 25-45, 45-65, 65-85, and 85-105 kyr b2k.

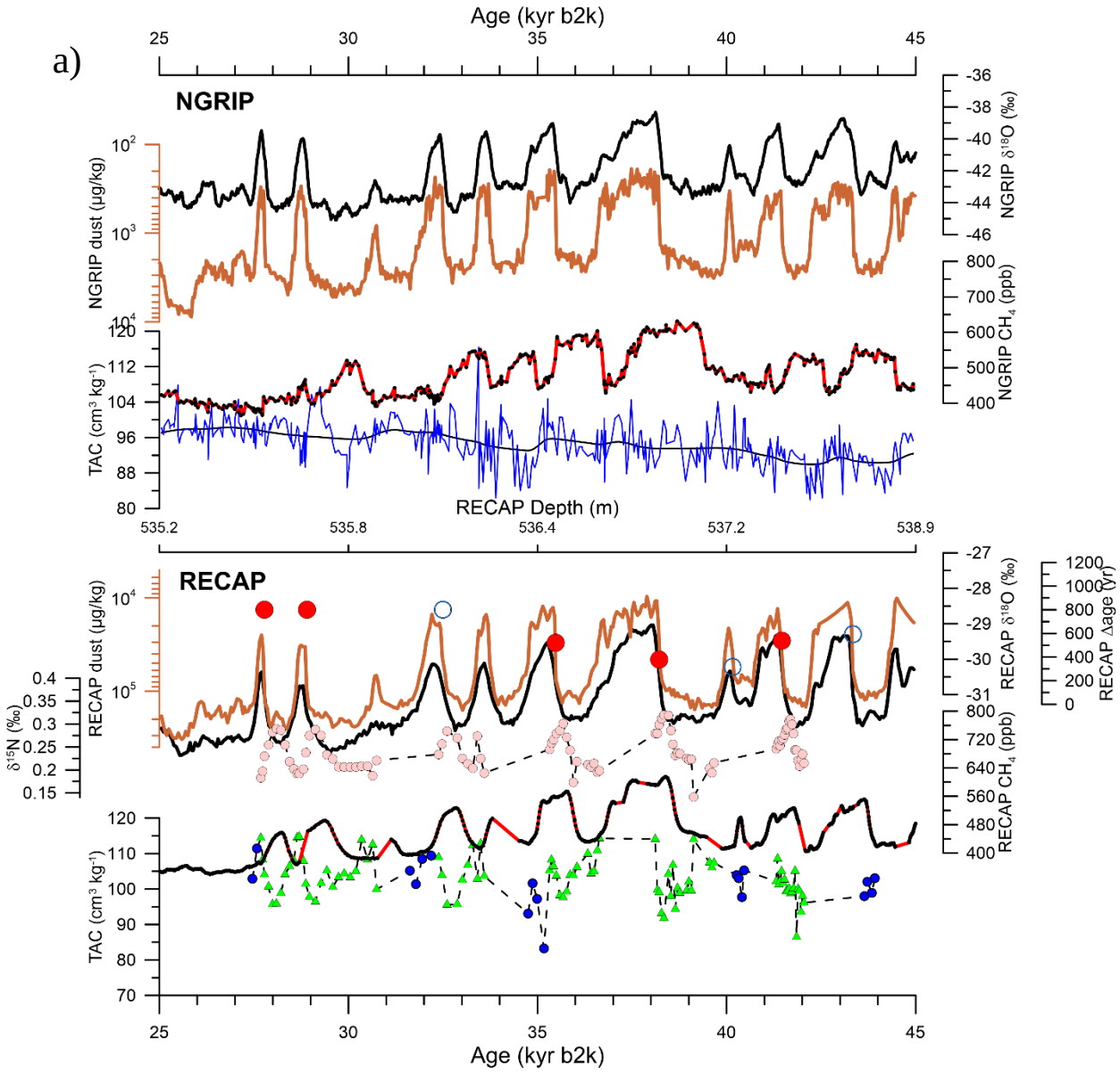

b)

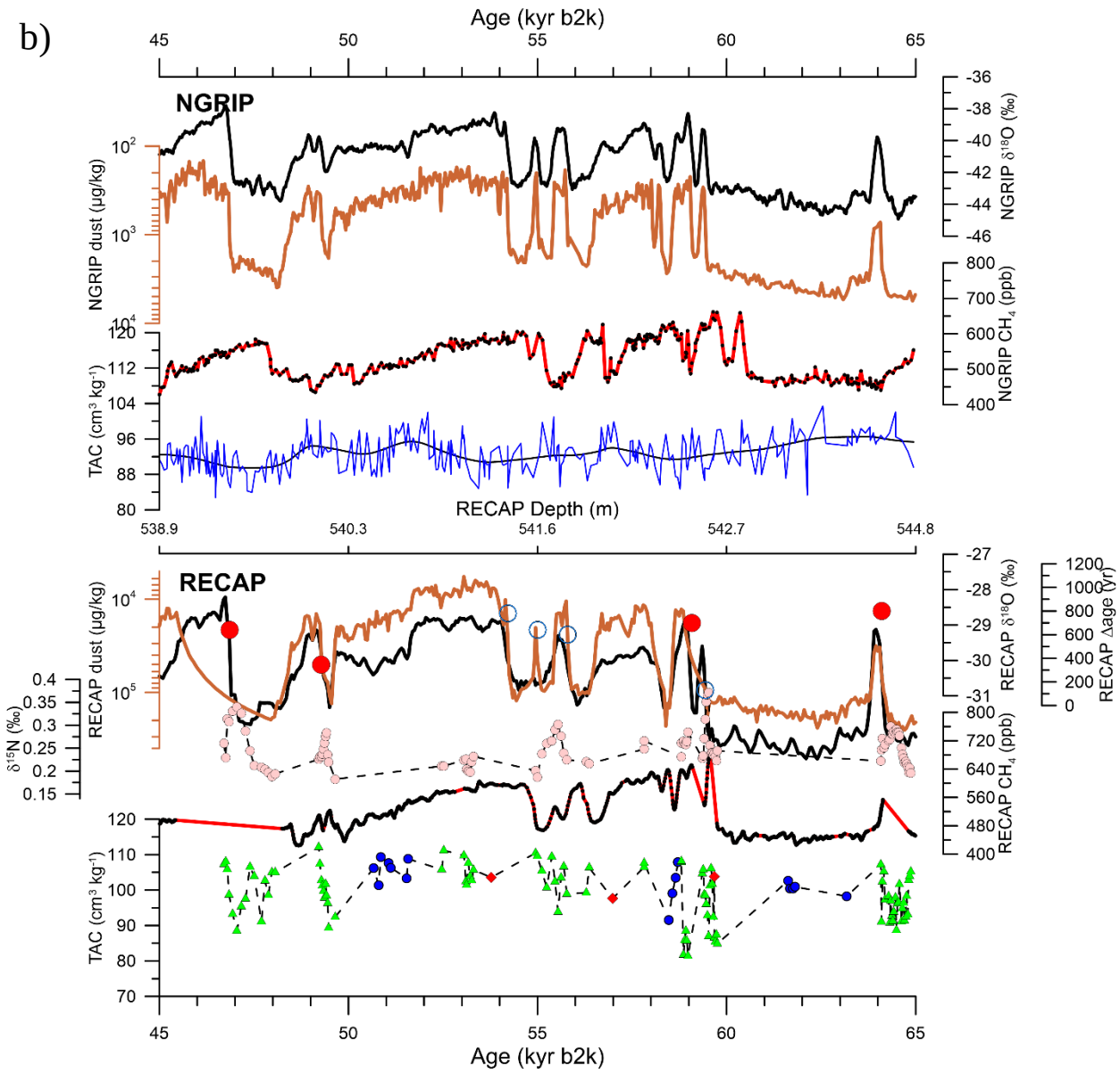
Age (kyr b2k)
45
50
55
60
65
NGRIP
NGRIP dust (µg/kg)
NGRIP δ18O (‰)
NGRIP CH4 (ppb)
TAC (cm3 kg-1)
RECAP Depth (m)
538.9
540.3
541.6
542.7
544.8
RECAP
RECAP dust (µg/kg)
δ15N (‰)
RECAP δ18O (‰)
RECAP CH4 (ppb)
RECAP Δage (yr)
Age (kyr b2k)

c)

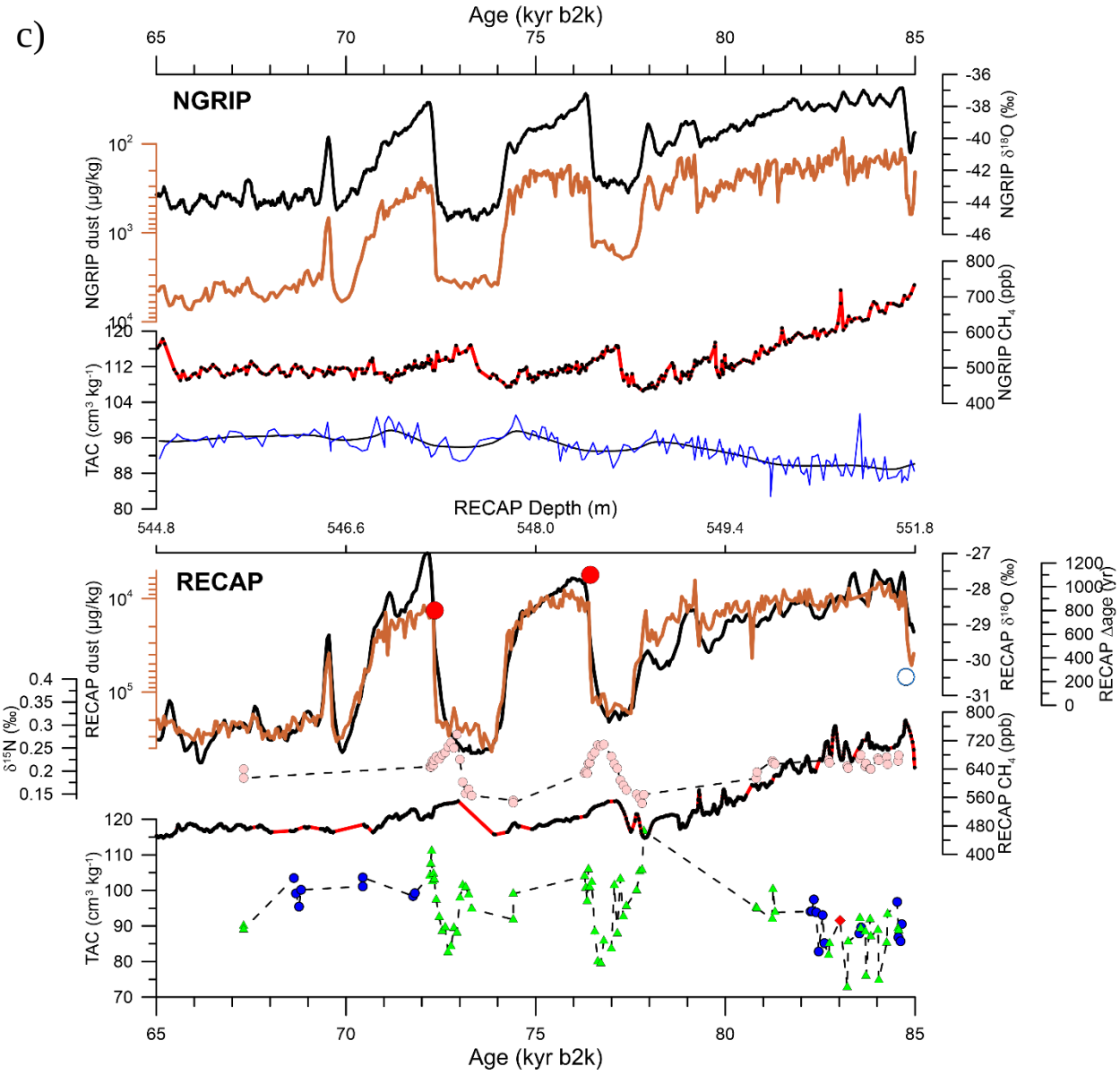
Age (kyr b2k)
65
70
75
80
85
NGRIP
NGRIP dust (µg/kg)
NGRIP δ18O (‰)
NGRIP CH4 (ppb)
TAC (cm3 kg-1)
RECAP Depth (m)
544.8
546.6
548.0
549.4
551.8
RECAP
RECAP dust (µg/kg)
δ15N (‰)
RECAP δ18O (‰)
RECAP CH4 (ppb)
RECAP Δage (yr)

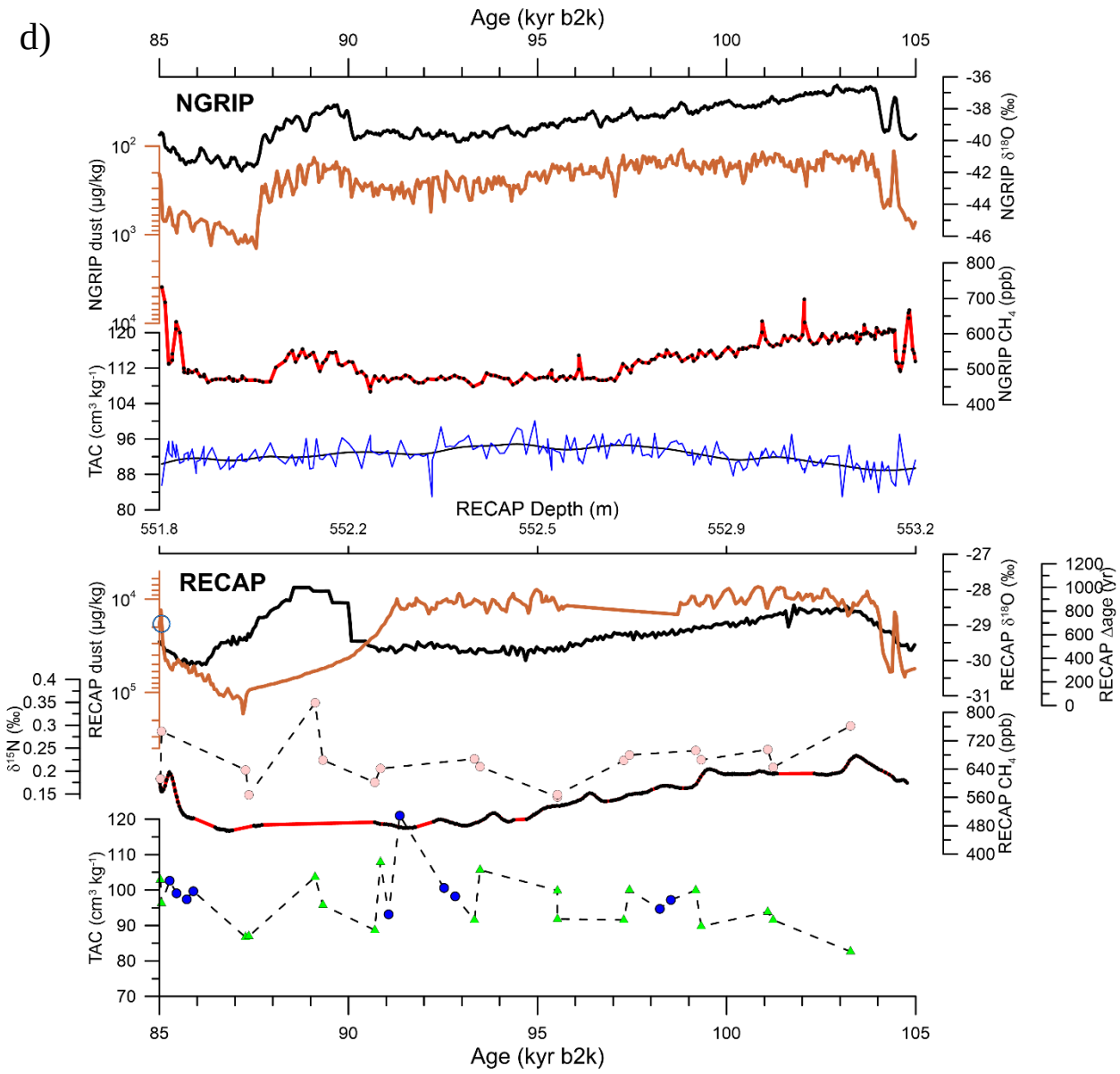

Figure S9 a to d: Glacial records from RECAP and NGRIP on their respective ice time scales: NGRIP top to bottom: water isotopes (black) (North Greenland Ice Core Project members, 2004), inverted dust (red) (Ruth et al., 2007), CH_4 (black dots and red line) (Baumgartner et al., 2014), TAC (blue line with spline fit in black) (Eicher et al., 2016). RECAP top to bottom water isotopes (black) (Gkinis et al., 2024), inverted dust (red) (Simonsen et al., 2019), Δage red dots and open circles for sections used and ignored for building the stacked records respectively (see section S5 for how Δage has been determined), $\delta^{15}N$ (pink), on-line CH_4 (black dots and red line, note that this data are not fully calibrated, concentrations are not absolute), TAC from PICE, PSU-CH_4, and PSU-$\delta^{15}N$ as blue dots, red diamonds, and green triangles, respectively.

S7.1 Variations associated with D-O events

We stacked the TAC data over D-O events to see the general features of the events. We did the same with the methane data and the $\delta^{15}N$ data. As lined out in the main text, dynamical effects in TAC can be expected from the moment of change till a new steady state is established. For the firn column this is when at a D-O event the higher accumulation snow has reached close off. As methane and temperature changes have been found to happen in close timely proximity (e.g. Baumgartner et al., 2014), the depth interval to be considered for a dynamical change is between the depth when methane changes are observed and the depth where changes in parameters recorded in the ice occur, e.g. $\delta^{18}O$ of H_2O or dust. This depth interval corresponds to Δage.

For the RECAP ice core, we have visually found Δage (and the corresponding depth interval) for the start of D-O events. We find that this depth interval corresponding to Δage (shown in Fig S9) is quite variable in RECAP. Why this is the case we do not know. We chose to produce a stacked plot over D-O events with normalized time axis. For each event the time axis is normalized so that the methane transition (in some events defined by change in $\delta^{15}N$) is set to 1 and the decrease in dust (coincident with the change in $\delta^{18}O$) is set to 0.

We treat the NGRIP dataset in a similar way making use of the Δage in Eicher et al. (2016) to define the interval. However, since in that publication Δage references the midpoint of methane transition while we used the start point for RECAP, we have assigned a value of 0.9 to the midpoint of the methane increase to make the NGRIP analyses compatible with our approach for RECAP.

Figures S10a and S10b show the result of this exercise for RECAP and NGRIP, respectively. For TAC, methane and $\delta^{15}N$, a lowpass cubic spline fit with a 200-year cutoff period, according to Enting (1987) with 1 sigma uncertainties for the spline fit is shown. Individual measurements for TAC (RECAP and NGRIP) and $\delta^{15}N$ (RECAP only) are plotted colour coded for the different D-O events. For RECAP open symbols indicate events that were excluded for the analyses where we have less than 10 TAC measurements for the event.

Methane data was also stacked and splined in a similar way. Apart from potential tiny modulations occurring in the trapping process the methane record of NGRIP and RECAP must be identical. However, the RECAP data has been analysed in a continuous flow setup resulting in smoothing of this highly compressed record. Nevertheless, the start of the events in CH_4 can be clearly identified. Note that this smoothing only applies to the RECAP CH_4 data. All other data are individual samples that do not suffer from smoothing effects during the analyses.

a)

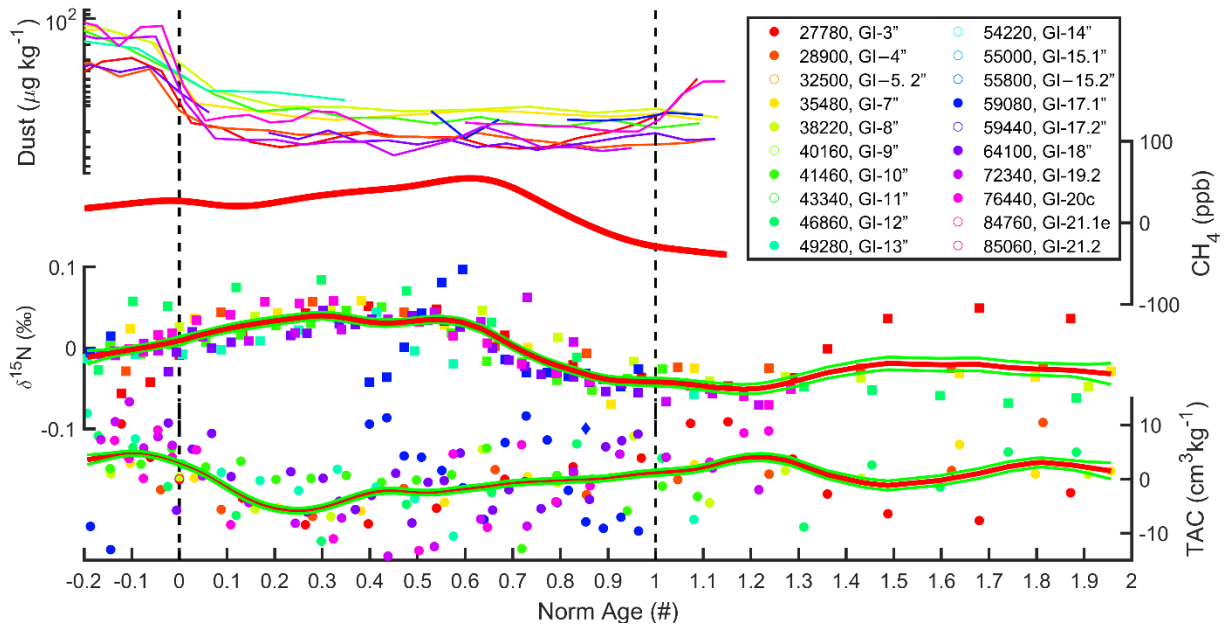

b)

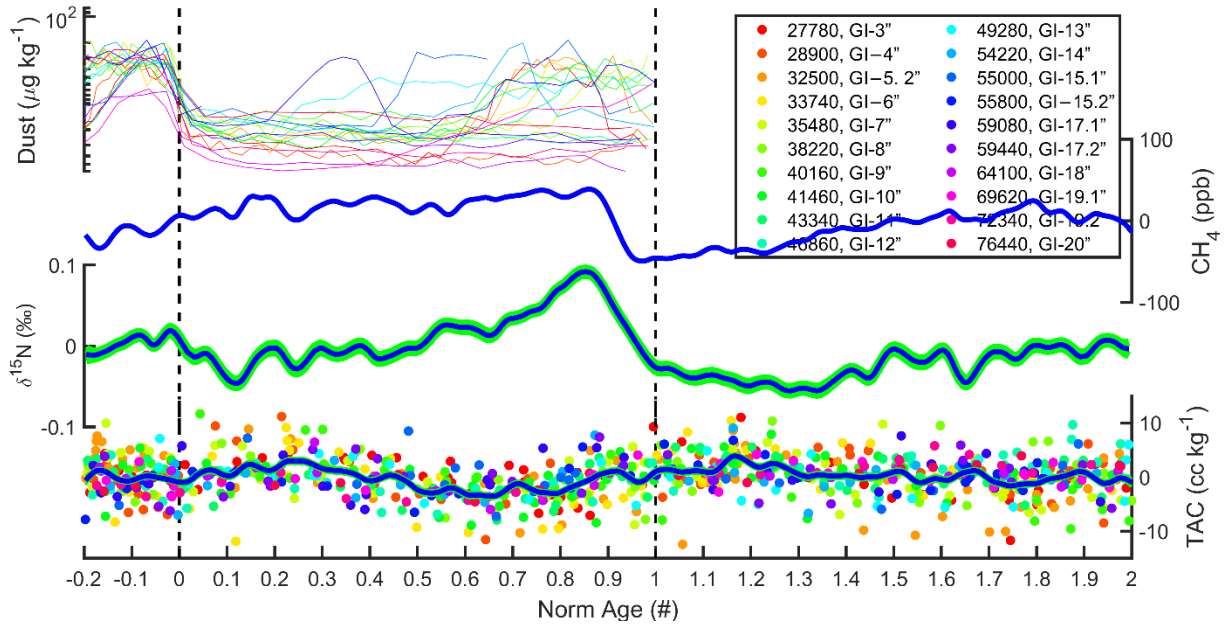

Figure S10 a) RECAP stacked record from top to bottom, dust, methane, $\delta^{15}N$, and TAC. Only events where there are more than 10 TAC samples available were considered. Events that are not included with open symbols in the legend. b) NGRIP stacked record from top to bottom, dust, methane, $\delta^{15}N$, and TAC.

S8 TAC and insolation

Following Eicher (2016, and references therein) we calculate the correlation between TAC and insolation. Like previous authors we chose an integrated local summer insolation (ISI) defined as the sum of insolation where the daily

insolation exceeds 380 W m^{-2}. While Raynaud et al. (2007) find high correlation of r^2 of 0.86 for Antarctic sites. The correlation for NGRIP is only 0.03 (Eicher et al., 2016). For RECAP the correlation becomes only 0.004 (Fig. S11) which leads us to speculate that the insolation effect may be depending on the accumulation rate. However, the higher variability associated with D-O events may explain part of the observed lower correlation.

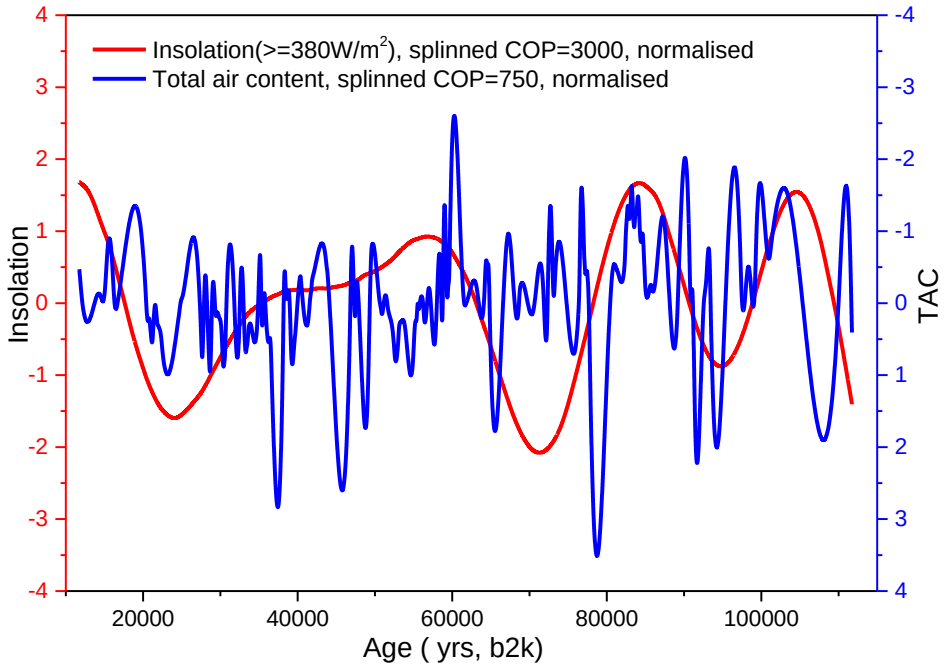

Figure S11: Insolation (≥ 380 W m^{-2}) signal for Renland, splined (COP=3000) and normalized in red, Glacial TAC signal of the RECAP core, splined (COP=750) and normalized in blue. The correlation of these signals is r^2=0.004.

References:

Aagaard, J.: Measurements of total air content of ice from EUROCORE, Greenland, Master thesis, Niels Bohr Institute, Faculty of Science, University of Copenhagen, 76 pp., 2015.

Baumgartner, M., Kindler, P., Eicher, O., Floch, G., Schilt, A., Schwander, J., Spahni, R., Capron, E., Chappellaz, J., Leuenberger, M., Fischer, H., and Stocker, T. F.: NGRIP CH_4 concentration from 120 to 10 kyr before present and its relation to a $\delta^{15}N$ temperature reconstruction from the same ice core, Clim Past, 10, 903-920, 10.5194/cp-10-903-2014, 2014.

Cappelen, J., Jørgensen, B. V., Laursen, E. V., Stannius, L. S., and Thomsen, R. S.: The Observed Climate of Greenland , 1958-99 - with Climatological Standard Normals , 1961-90 Klimaobservationer i Grønland , 1958-99, Danish Meteorological Institute, CopenhagenISSN 1399-1388, 151, 2001.

Eicher, O., Baumgartner, M., Schilt, A., Schmitt, J., Schwander, J., Stocker, T. F., and Fischer, H.: Climatic and insolation control on the high-resolution total air content in the NGRIP ice core, Clim. Past, 12, 1979-1993, 10.5194/cp-12-1979-2016, 2016.

Enting, I. G.: On the use of smoothing splines to filter CO_2 data, J Geophys Res-Atmos, 92, 10977-10984, 10.1029/JD092iD09p10977, 1987.

Fegyveresi, J. M.: Physical properties of the West Antarctic Ice Sheet (WAIS) Divide deep core: Development, evolution, and interpretation, Ph.D. thesis, Department of Geosciences, The Pennsylvania State University, Ann Arbor, 304 pp., 2015.

Gkinis, V., Vinther, B. M., Cook, E., Freitag, J., Holme, C. T., Hughes, A. G., Kipfstuhl, S., Kjær, H. A., Maffrezzoli, N., Morris, V., Popp, T. J., Rasmussen, S. O., Simonsen, M. F., Svensson, A. M., Vallelonga, P. T., Vaughn, B. H., White, J. W. C., Winstrup, M., and Hansen, S. B.: An ultra-high resolution water isotope record ($\delta^{18}O$, δD)

from the Renland ice cap spanning 120,000 years of climate history, Pangaea, doi.pangaea.de/10.1594/PANGAEA.966693, 2024.
Lipenkov, V., Candaudap, F., Ravoire, J., Dulac, E., and Raynaud, D.: A New Device for the Measurement of Air Content in Polar Ice, Journal of Glaciology, 41, 423-429, 1995.
Martinerie, P., Lipenkov, V., and Raynaud, D.: Correction of air content measurements in polar ice for the effect of cut bubbles at the surface of the sample, Journal of Glaciology, 36, 299-303, Doi 10.3189/002214390793701282, 1990.
Martinerie, P., Lipenkov, V. Y., Raynaud, D., Chappellaz, J., Barkov, N. I., and Lorius, C.: Air content paleo record in the Vostok ice core (Antarctica): A mixed record of climatic and glaciological parameters, J Geophys Res-Atmos, 99, 10565-10576, 10.1029/93jd03223, 1994.
North Greenland Ice Core Project members: High-resolution record of Northern Hemisphere climate extending into the last interglacial period, Nature, 431, 147-151, 10.1038/nature02805, 2004.
Raynaud, D., Lipenkov, V., Lemieux-Dudon, B., Duval, P., Loutre, M. F., and Lhomme, N.: The local insolation signature of air content in Antarctic ice. A new step toward an absolute dating of ice records, Earth Planet Sc Lett, 261, 337-349, 10.1016/j.epsl.2007.06.025, 2007.
Ruth, U., Bigler, M., Röthlisberger, R., Siggaard-Andersen, M.-L., Kipfstuhl, S., Goto-Azuma, K., Hansson, M. E., Johnsen, S. J., Lu, H., and Steffensen, J. P.: Ice core evidence for a very tight link between North Atlantic and east Asian glacial climate, Geophys Res Lett, 34, 10.1029/2006GL027876, 2007.
Sander, R.: Compilation of Henry's law constants (version 4.0) for water as solvent, Atmos. Chem. Phys., 15, 4399-4981, 10.5194/acp-15-4399-2015, 2015.
Schwander, J.: Lufteinschluss im Eis von Grönland und der Antarktis, PhD thesis, Universität Bern, 1984.
Simonsen, M. F., Baccolo, G., Blunier, T., Borunda, A., Delmonte, B., Frei, R., Goldstein, S., Grinsted, A., Kjaer, H. A., Sowers, T., Svensson, A., Vinther, B., Vladimirova, D., Winckler, G., Winstrup, M., and Vallelonga, P.: East Greenland ice core dust record reveals timing of Greenland ice sheet advance and retreat, Nature Communications, 10, 10.1038/s41467-019-12546-2, 2019.